Mechanical characterisation of the developing cell wall layers of tension wood fibres by Atomic Force Microscopy

O. Arnould[1], M. Capron[1a], M. Ramonda[2], F. Laurans[3], T. Alméras[1], G. Pilate[3], B. Clair[1]

Running title: Mechanical properties of developing secondary wall by AFM

[1] LMGC, Univ. Montpellier, CNRS, Montpellier, France

[2] CTM, Univ. Montpellier, Montpellier, France

[3] INRAE, ONF, BioForA, Orléans, France

olivier.arnould@umontpellier.fr

Date of submission:

Number of tables: 1

Number of figures: (colour in print) 9

Word count (start of the introduction to the end of the acknowledgements, excluding materials and methods): 5656

Supplementary data number of figures, tables or videos: 3 figures

[a] Now at: Partnership for Soft Condensed Matter PSCM, ESRF The European Synchrotron Radiation Facility, Grenoble, France

Highlight

New insights into the changes in mechanical properties within the cell wall of poplar tension wood fibres during maturation have been obtained using atomic force microscopy.

Abstract

Trees can generate large mechanical stresses at the stem periphery to control the orientation of their axes. This key factor in the biomechanical design of trees, named "maturation stress", occurs in wood fibres during cellular maturation when their secondary cell wall thickens. In this study, the spatial and temporal stiffening kinetics of the different cell wall layers were recorded during fibre maturation on a sample of poplar tension wood using atomic force microscopy. The thickening of the different layers was also recorded. The stiffening of the CML, S_1 and S_2-layers was initially synchronous with the thickening of the S_2 layer and continued a little after the S_2-layer reached its final thickness as the G-layer begins to develop. In contrast, the global stiffness of the G-layer, which initially increased with its thickening, was almost stable long before it reached its final maximum thickness. A limited radial gradient of stiffness was observed in the G-layer, but it decreased sharply on the lumen side, where the new sub-layers are deposited during cell wall thickening. Although very similar at the ultrastructural and biochemical levels, the stiffening kinetics of the poplar G-layer appears to be very different from that described in maturing bast fibres.

Keywords

Atomic Force Microscopy; Cell wall; G-layer; Indentation modulus; Maturation; Poplar; Stiffening; Tension wood; Thickening.

Abbreviations

AFM: Atomic force microscopy

PF-QNM: Peak-force quantitative nano-mechanics

MFA: Microfibril angle

Introduction

Wood fibres have mechanical functions in the living tree. Mature wood fibres give the tree axis sufficient stiffness and strength to withstand its own weight and additional loads such as wind or fruits (Niklas, 1992). In addition to this "skeletal" function, wood fibres also have a "muscular" function to control the posture of the tree by actively generating forces that can bend the stem upwards or compensate for the effect of gravity (Alméras and Fournier, 2009; Alméras *et al.*, 2018; Fournier *et al.*, 2014; Moulia *et al.*, 2006; Scurfield, 1973). During their maturation, wood fibre cell walls undergo significant physico-chemical changes that would result in major deformation if they were not prevented by the older, stiff tissue, surrounding them. In place of strain, this leads to the development of a high mechanical stress named "maturation stress". Maturation stress is particularly high in reaction wood (Archer 1986), a specialised tissue produced by the tree in response to mechanical disturbance. In angiosperms, reaction wood is called tension wood because its maturation stress tension is high, of the order of several tens of MPa. Tension wood acts like muscle by pulling on one side of the stem, thereby enabling its reorientation (Okuyama *et al.*, 1994; Yamamoto, 1998). Mechanical stress is known to be generated in a specific cell wall layer of tension wood fibres, named the G-layer (Côté *et al.*, 1969; Dadswell and Wardrop, 1955; Fang *et al.*, 2008; Ghislain and Clair, 2017; Onaka, 1949). However, the mechanisms responsible for the generation of high tensile stress during G-layer maturation are still the subject of debate. Several hypothetical models have been proposed, which are reviewed in Alméras and Clair (2016). Gaining knowledge on the chemical, physical and mechanical states of the material and their changes during cell wall maturation have proven particularly useful in distinguishing between these models. For example, it has been observed that the G-layer contains mesopores of several nanometres (Chang *et al.*, 2009; Clair *et al.*, 2008), and that these pores swell during maturation (Chang *et al.*, 2015). It has also been shown that crystalline microfibrils are under tension during maturation (Clair *et al.*, 2011). The synchronicity between these two phenomena supports the hypothesis that pore swelling is related to the induction of maturation stresses in the G-layer (Alméras and Clair, 2016).

A crucial factor is the change in cell wall stiffness during maturation. Indeed, using mechanical modelling, it has been shown that the relative kinetics of stiffening and stress induction affect the resulting state of stress in the tree (Alméras *et al.*, 2005; Pot *et al.*, 2014; Thibaut *et al.*, 2001). As reported by Thibaut *et al.* (2001), the tendency of the material to deform in response to physico-chemical changes can result in stress of high magnitude only if the cell wall is already sufficiently stiff. To the best of our knowledge, information on the stiffening dynamics of (tension) wood cell wall layers is currently lacking and the only measurements available are at the tissue scale (Grozdits and Ifju, 1969; Pot *et al.*, 2013a; 2013b).

One of the most promising and frequently used techniques today, nanoindentation, probes the mechanical properties at the cell wall scale. It enables access to the mechanical properties within the cell wall layers with modifications reduced to a minimum. This technique has already been used to estimate the indentation modulus of mature native or thermo-mechanically modified cell walls of wood fibres (Eder *et al.*, 2013), lignifying spruce tracheid secondary cell walls (Gindl *et al.*, 2002) and (thick) fibre cell walls within a maturing vascular bundle of bamboo (Wang *et al.*, 2012; Huang *et al.*, 2016). However, as widely recognized in the case of metal materials, the radius of the plastically affected volume around the indenter is about three times the residual indent size for an isotropic material and even more for the elastically affected one (Johnson 1987; Sudharshan Phania and Oliver, 2019). This technique therefore requires a layer thickness at least three times the size of the indent, which are typically in the micrometre range, to avoid measurement artefacts (Jakes *et al.*, 2009). As the width of the cell wall layers in the developing and maturation stages vary from almost zero (cambium, beginning of the layer deposition) to a few micrometres (mature S_2 and/or G-layer), interpreting the measurements obtained by nanoindentation in the presence of a gradient of properties or within a thin layer is not straightforward, nor possible close to the cambium, due to boundary effects. In such cases, atomic force microscopy (AFM) appears to be the best way to perform mechanical measurements within each cell wall layer (Arnould and Arinero, 2015; Casdorff et al., 2017; 2018; Clair *et al.*, 2003, Coste *et al.*, 2021; Nair *et al.*, 2010; Normand *et al.*, 2021). This technique has already been used to investigate, for example, the development of bast fibres within a flax stem (Goudenhooft *et al.*, 2018) and of the primary cell walls in the inner tissues of growing maize roots (Kozlova *et al.*, 2019).

The aim of the present work was to measure changes in the indentation modulus of each cell wall layer during the maturation of poplar tension wood fibres using AFM. As it was not possible to monitor the maturation of a single cell over time, as a proxy, we chose to perform measurements on several cells in the same row, from cambium to mature wood, that were therefore at different stages of development. Using the kinetics of cell wall thickening as a basis for comparison, the stiffening of the different layers of the cell wall was compared to other known phenomena such as changes in mesoporosity and in crystalline cellulose strain. In addition, thanks to the nanometric spatial resolution of AFM measurements, we investigated G-layer stiffening during thickening, i.e., the kinetics of stiffening within the G-layer, and fluctuations in the mechanical states of a new freshly deposited sub-layer. Finally, the kinetics and stiffness gradient of the poplar G-layers were compared with data available in the literature on bast (primary phloem) and xylem flax fibres, whose cells walls contain both a thick immature G_n-layer and a mature G-layer (Goudenhooft *et al.*, 2018; Petrova *et al.*, 2021).

Materials and methods

Sample preparation

The experiments were conducted on a wood sample cut out of a young poplar tree tilted to induce the production of tension wood. This hybrid poplar plant (*Populus tremula* × *Populus alba*, INRA clone 717-1-B4), was grown in controlled greenhouse conditions for two months (INRAE, Orléans, France) before being tilted to trigger the formation of tension wood on the upper side of its stem. Twenty-two days after tilting, a 5-cm long stem section (estimated diameter 1 cm) was collected at the base of the stem, a few cm above the ground. Small wood sub-samples a few mm in size were cut out of the tension wood side and fixed for 4 h in 2.5% formaldehyde and 0.1% glutaraldehyde in 0.1M McIlvaine citrate-phosphate buffer, pH 6.8, followed by 3×10 min under moderate vacuum. After thorough rinsing in McIlvain buffer, the sample was partially dehydrated in increasing series (25%, 50%, 70%) of ethanol and progressively impregnated with LR-White medium grade resin (London Resin Company Ltd, UK) in a series of resin and ethanol mixes containing a progressively increasing percentage of resin (20% 2h, 40% 4h, 60% 4h, 80% 24h, 100% 2+8 days). During the last pre-embedding step, in pure resin, the sample was placed under moderate vacuum for 3×10 minutes. Finally, the samples were embedded in gelatine capsules filled with pure resin and heated in an oven at 56 °C for 24 h for polymerization. Semi-thin transverse sections (0.5 to 1 µm) were cut with a Histo diamond knife (Diatome Ltd, Nidau, Switzerland) installed on a Ultracut S microtome (Leica Microsystems, Vienna, Austria) to trim the block. To avoid the deformation commonly observed in G-layers as a result of swelling, detachment and collapse after stress release (Clair *et al.*, 2005a; 2005b), at least the first 50 µm of the sample were trimmed and discarded. Finally, very thin sections (about 50 nm thick in the last step) were made at a low cutting speed (≈1 mm/s) using an Ultra AFM diamond knife (Diatome) to obtain a nearly perfect flat surface. AFM measurements were carried out on the remaining block.

Optical measurement of the cell wall layer thickness

After AFM experiments, semi-thin transverse sections (0.9 µm) were cut with a Histo diamond knife (Diatome) installed on an Ultracut R microtome (Leica Microsystems). These sections were stained using Richardson's azur II and methylene blue (Richardson *et al.*, 1960) and mounted on slides using Canada balsam. The slides were observed under a light microscope (DMLP, Leica Microsystems) with immersion oil lenses (Fig. 1). Phase contrast microscopy is preferable to bright field microscopy when observing the cell wall layer with high magnification (×600) as the specimen is thin, so the colour contrast is reduced (Abedini *et al.*, 2015). Several images were acquired using a light microscope with a digital camera (DFC320, Leica Microsystems) from the cambium to a distance of

about 2 mm from it on the xylem side (i.e., with fully matured fibres), with a sufficient overlap to allow the image to be repositioned to accurately measure the distance of each cell from the cambium. The mean thickness of the S_2 and G layers was measured all along two radial rows using Matlab software (MathWorks Inc., Natick, Massachusetts, USA) according to the method of Yoshinaga *et al.* (2012). External contours of the lumen, S_2 and G layers were plotted by hand from images and their average thickness was calculated as (Abedini *et al.*, 2015):

$$Th_G = \frac{2A_G}{P_G + P_{lumen}}, \tag{2}$$

$$Th_{S2} = \frac{2A_{S2}}{P_{S2} + P_G}, \tag{3}$$

where A_G and P_G are the area and the external perimeter of G-layer, respectively, A_{S2} and P_{S2} are the area and the external perimeter of the S_2 layer, respectively, and P_{lumen} is the lumen perimeter. The data presented in this article show the thickness of each layer normalized by the mean cell diameter, D, which was evaluated as $D = \frac{P_{S2}}{\pi}$. The advantage of working with relative thickness is that it allows the effect of the fibre ends on the cell wall thickness to be corrected (Okumura *et al.*, 1977; Abedini *et al.*, 2015).

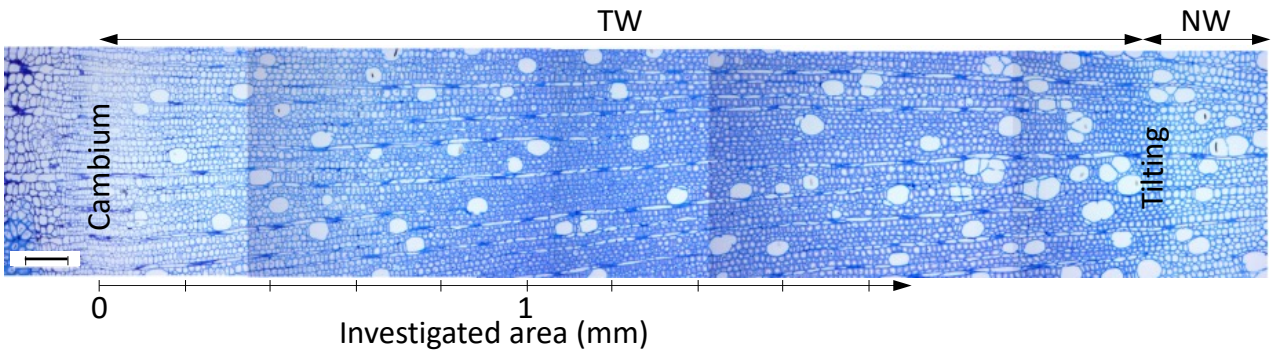

Fig. 1. Optical image of the transverse section of the wood sample (Richardson's staining) with the tension wood (TW) area between the cambium and the normal wood (NW) produced before the tree was tilted. The reference distance from the cambium was measured approximately in the middle of the cambial zone. Scale bar = 0.1 mm.

AFM PF-QNM measurements

Mechanical characterisation was performed with a Multimode 8 AFM (Bruker Corporation, USA) in PF-QNM imaging mode with a RTESPA-525-30 (Bruker) probe. The spring constant of the probe was calibrated by Bruker using a laser Doppler vibrometer with a value of 158 N/m. The initial tip

radius, 33 nm (controlled by Bruker), was checked after adjusting the cantilever deflection sensitivity on sapphire and corrected to 40 nm to obtain the right range of indentation modulus on the centre of DuPont™ K48 Kevlar® fibres (~20 GPa) embedded in Struers Epofix epoxy resin (~4 GPa), as described in Arnould *et al.* (2017). The value of the tip radius was checked indirectly and, if necessary, corrected using the above-mentioned calibration sample by ensuring that the indentation modulus and the adhesion force in the embedding resin of the wood sample remained constant around the wood sample and within the lumen in the cambial area. After all the measurements, the final tip radius was 120 nm. The applied maximum load was set at 200 nN for all the measurements, the vertical motion for force-distance curves was set at a frequency of 2 kHz, and the fast scan rate was such that the scan speed was always equal to 8 µm/s regardless of the size of the image (512 × 512 pixels), with a scan axis angle of 90°.

The force-distance curves obtained were automatically adjusted by a Derjaguin-Muller-Toporov (DMT) contact model (Derjarguin *et al.*, 1975) to obtain the indentation modulus using Nanoscope Analysis software (Bruker), with an assumed spherical tip, a flat sample surface, and taking the measured adhesion force into account. This model is one of the simplest and is suitable for vitreous polymer resin and all wood cell wall layers, considering the relatively low values of their Tabor parameter (Johnson and Greenwood, 1997; Xu *et al.*, 2007). The discernible layers, i.e., layers that are thick enough to avoids the measurement being influenced by edge or topography effects, are the cell corner middle lamella (CCML), S_1 with the primary wall (i.e., S_1-P, as in most cases, these two layers are almost impossible to distinguish), S_2 and G layers. For each of these layers, the indentation modulus distribution was obtained using Gwyddion freeware (http://gwyddion.net/). This distribution can be adjusted with a Gaussian function that gives the value at the maximum of the distribution (i.e., mode or most frequent value in the dataset) and the standard deviation of the indentation modulus. Measurements were made on three different radial rows of developing cells in the wood sample, one after the other, always starting from the cambium and continuing up to a distance of about 1.7 mm away, with two overlapping sets of measurements for the first row to check the stability and repeatability of the measurements. Twenty-four different positions (and thus cells) were measured in the two first radial rows and 12 positions in the last row. As soon as it was visible, the thickness of the S_2 and G layers was measured using the same protocol as for the optical images. To complete our study and to have a reference, we measured the indentation modulus and the thickness of the cell wall layers in three normal wood cells (one per radial row) that had differentiated before the tree was tilted and were therefore devoid of a G-layer. All the data were assembled using Matlab software (The MathWorks Inc., Natick, Massachusetts, USA).

Finally, the AFM values were checked by nanoindentation measurements on a few cells located 700 µm from the cambium using iNano KLA nanoindenter (Scientec, Les Ulis, France) in mapping mode (NanoBlitz) on a 200 × 200 µm (20 × 20 pixels) area, with a maximum force of 0.1 mN and a loading frequency of 1 Hz.

Results

Mapping the indentation modulus of developing fibres

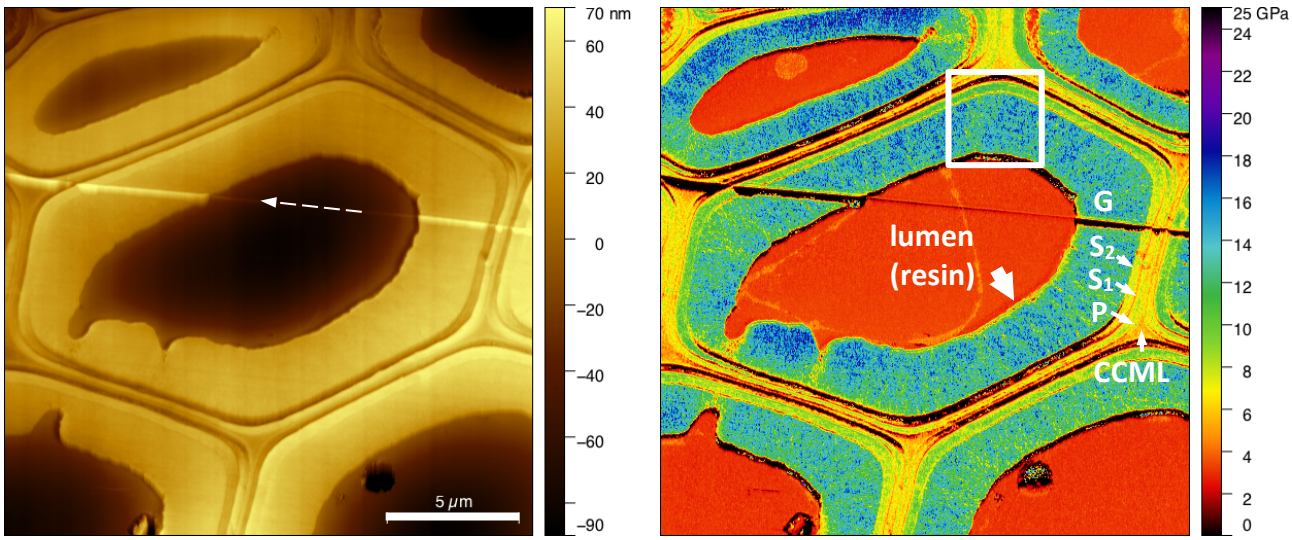

(a) *(b)*

Fig. 2. PF-QNM mapping of (a) topography and (b) indentation modulus of the cross section of a tension wood fibre 740 µm from the cambium (first radial row). The different layers are identified: P stands for primary wall and CCML for cell corner middle lamella. The lumen of the cell was filled with LR-White resin. The white dashed arrow in (a) shows the microtome cutting direction (following a scratch line due to imperfections of the diamond knife), the thick white arrow in (b) points to a thin and softer sub-layer that corresponds to the white upper box in (b) and is discussed in more detail in Fig. 4.

The AFM measurements provided a map of the sample topography and a map of the indentation modulus. Examples of typical maps obtained for a cell are given in Fig. 2, at a distance of 740 µm from the cambium (first radial row). The different layers of the cell wall (cell corner middle lamella CCML, primary cell wall P, secondary cell wall S_1, S_2 and G-layers) are clearly identifiable on the indentation modulus map due their different elastic mechanical properties. Note that part of the cell contents in the lumen are identifiable (Fig. 2b), while they are not visible in the topography (Fig. 2a). The different cell wall layers are also quite easy to distinguish on the topography map because of the

slight change in height between each layer. The height is almost uniform within the G-layer, middle lamella and embedding resin in the lumen, whereas it varies around the circumference in the S_1-P and S_2 layers. These variations are the opposite in the S_1-P and S_2 (S_1-P is high when S_2 is low) and these extreme values were obtained perpendicular to the cutting direction (white dashed arrow in Fig. 2a). These observations are typical of a cutting effect as previously described in Arnould and Arinero (2015). Moreover, we observed limited orthoradial variations in the indentation modulus of the S_2-layer around the cells. This proves that the wood fibres are rather well oriented perpendicular to the cutting direction and that there will be little (or even no) bias in the interpretation of the measurements due to sample misalignment (Arnould and Arinero, 2015).

Fig. 3 shows the mechanical maps of all the cells measured in the first radial row. Progressive thickening of the cell wall results in the appearance of the different layers of the secondary wall: the first distinguishable S_2 appears around 50 µm from the cambium (map with the green border in Fig. 3) and first distinguishable G-layer around 230 µm from the cambium (map with the blue border in Fig. 3). A continuous increase in the indentation modulus of the embedding resin is visible in the lumen from 2.7±0.1 GPa in the cambium to 3.4±0.2 GPa at 1.7 mm. This increase was not observed in the embedding resin outside the wood sample where the indentation modulus remained equal to around 2.7±0.1 GPa in all the measurements. Moreover, immediate measurement of the indentation modulus of the embedding resin in the lumen of cells in the cambium taken just after the last measured cell in a given row, showed a return the initial value of 2.7±0.1 GPa.

The indentation modulus obtained for the S_2-layer of normal wood cells 2 mm from the cambium, was around 16.9±5.5 GPa and its relative thickness was around 0.055 (see NW in Fig.3). A more pronounced variation of the indentation modulus was observed in the S_2-layer of this cell, which is probably due to a slight misorientation of the fibre with respect surface as already described in Arnould and Arinero (2015). The indentation moduli of the other layers were 7.5±1.2 for the CCML and 8.2±3.1 GPa for the S_1-layer, while the indentation modulus in the embedding resin in the lumen was 2.99±0.21, a value close to that recorded in the cambium or outside the wood sample. The indentation modulus was confirmed by nanoindentation in the embedding resin in the lumen and in the G-layer of a few cells 700 µm from the cambium with a value of 3.5±0.15 GPa and 13.5±1.3 GPa, respectively (see Fig. S3 and Table 1 for comparison).

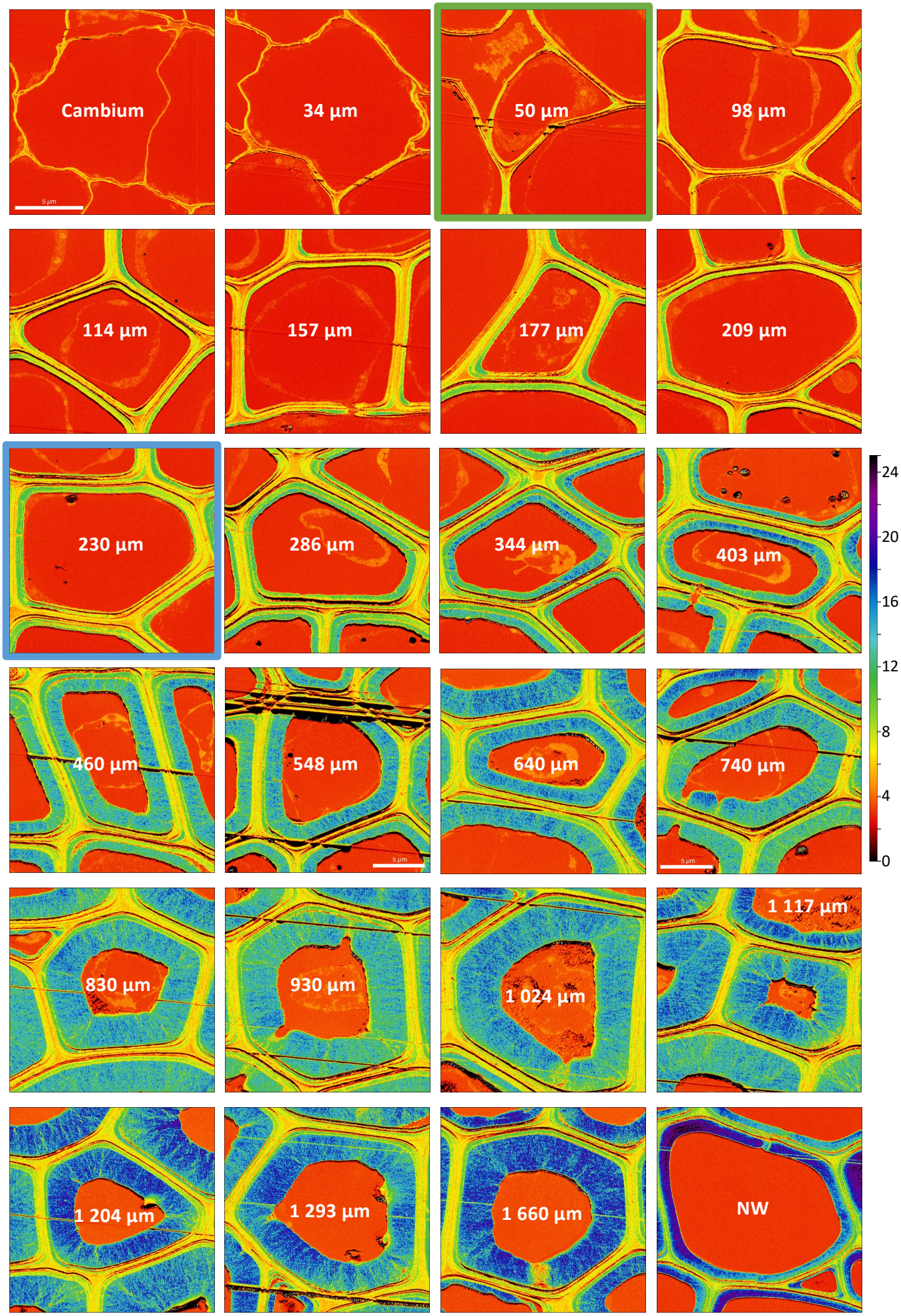
Cambium
34 µm
50 µm
98 µm
114 µm
157 µm
177 µm
209 µm
230 µm
286 µm
344 µm
403 µm
460 µm
548 µm
640 µm
740 µm
830 µm
930 µm
1 024 µm
1 117 µm
1 204 µm
1 293 µm
1 660 µm
NW
24
20
16
12
8
4
0

262

Fig. 3. Indentation modulus maps of the different cells measured in the first radial row. The white number in the lumen refers to the distance of the cell from the cambium, the cells are arranged in rows from left to right and from top to bottom, with the cambium always on the left. The last map on the bottom right shows a normal wood (NW) cell, here before tilting (Fig. 1). The map at 50 µm (green border) is the first map with a distinguishable S_2-layer. The map at 230 µm (blue border) is the first map with a distinguishable G-layer. Except for the maps at 548 and 740 µm, the size of the maps is same in all the images. Scale bar = 5 µm.

Overall stiffening of the G-layer with increased distance from the cambium was clearly visible. A radial pattern (radial lines in the cell wall) was also visible in the G-layer, as previously reported by Sell and Zimmermann (1998). Some ring lamellae were also visible within the cell wall layers (e.g., at 548, 740, 830, 930, 1024 and 1660 µm from the cambium in Fig. 3 and in the enlargement of Fig. 2b in Fig. S1). This last structural pattern is consistent with the radial layer-by-layer thickening of the wall and has been already reported, for example, in the S_2-layer of wood fibres (Fahlén and Salmén, 2002; Casdorff *et al.*, 2018), in the G-layer of most *Salicaceae* species excepted in the poplar genera (Ghislain *et al.*, 2016), in mature (Hock, 1942) and in developing G-layers of flax bast fibres (Arnould *et al.*, 2017; Goudenhooft *et al.*, 2018) and in mature hemp fibres with a G-layer (Coste *et al.*, 2020).

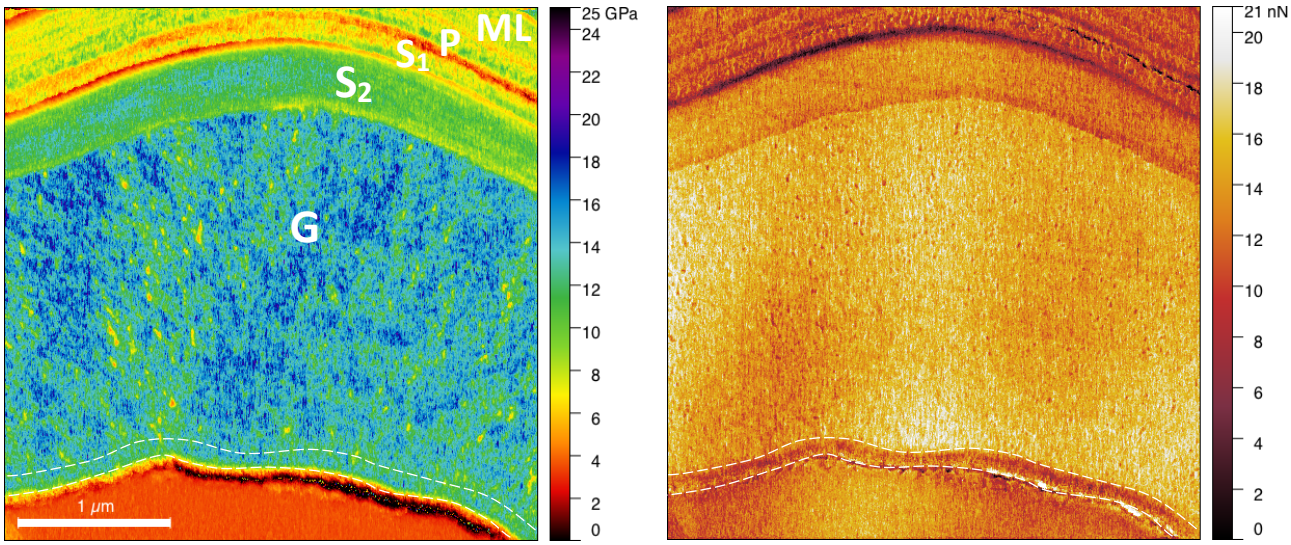

(a) *(b)*

Fig. 4. a) Close-up of the indentation map of a cell taken at a distance of 740 µm from the cambium corresponding to the white box in Fig. 2b with the associated adhesion map (b) highlighted sub-G-layer with lower adhesion force close to the lumen.

At a distance from the cambium equal to or greater than 440 µm, a thin and soft sub-layer was visible on the lumen side at the border of the G-layer but only on the right side of the map (as shown in Fig. 2b). The fact that this sub-layer is only visible on the right side of all cells can be attributed to a cutting effect when the sample surface was prepared with the diamond knife, as the cutting direction is almost horizontal and proceeds from the right to the left (see Fig. 2a). As cutting effects are linked to the mechanical behaviour of the cell wall, this sub-layer reveals a different behaviour than the rest of the G-layer. The average indentation modulus of this sub-layer was around 8.2±2.6 GPa, close to the value of the early G-layer, at a distance of 230-286 µm from the cambium, and its thickness was around 100 nm in all cases. Fig. 4a gives a closer view of the G-layer at the top of the cell at 740 µm from the cambium (white box in Fig. 2b) and Fig. 4b is the adhesion map. Although the sub-layer is not visible on the indentation map in Fig. 4a, a sub-layer with a thickness of around 100 nm and a lower adhesion force than the rest of the G-layer is also visible on the border of the lumen in Fig. 4b. We can assume that it is the same sub-layer as that observed on the right side of the indentation modulus maps. Moreover, its low adhesion force is close to that of the early G-layer (see Fig. S2).

To further investigate the kinetics of G-layer stiffening, from six fibres situated at different distances from the cambium, we extracted six to ten radial profiles of the indentation modulus around the cell axis in the G-layer (Fig. 5). Each point in a radial profile is the average of the modulus over a width of 10 pixels. To reduce possible bias in the interpretation of the data caused by an edge effect due to cutting with the diamond knife or an effect of the area mechanically sensed by the tip (Sudharshan Phani and Oliver, 2019), we removed the first and last 100 nm from each profile (data points in grey in Fig. 5). In contrast to the indentation modulus map in Figs. 2b and 3, where no mechanical gradient is visible in the developing G-layers, here a gradient was always visible on the last 500 nm or so on the lumen side and became less pronounced with an increase in the distance from the cambium. The gradient completely disappeared in the mature fibre (see Fig. 5 at 1 660 µm). It was not possible to determine whether such a gradient existed in the S_2-layer because, even if it were present, it would be hidden by the effect of the apparent microfibril angle due to the slight misalignment of the sample (Arnould and Arinero, 2015).

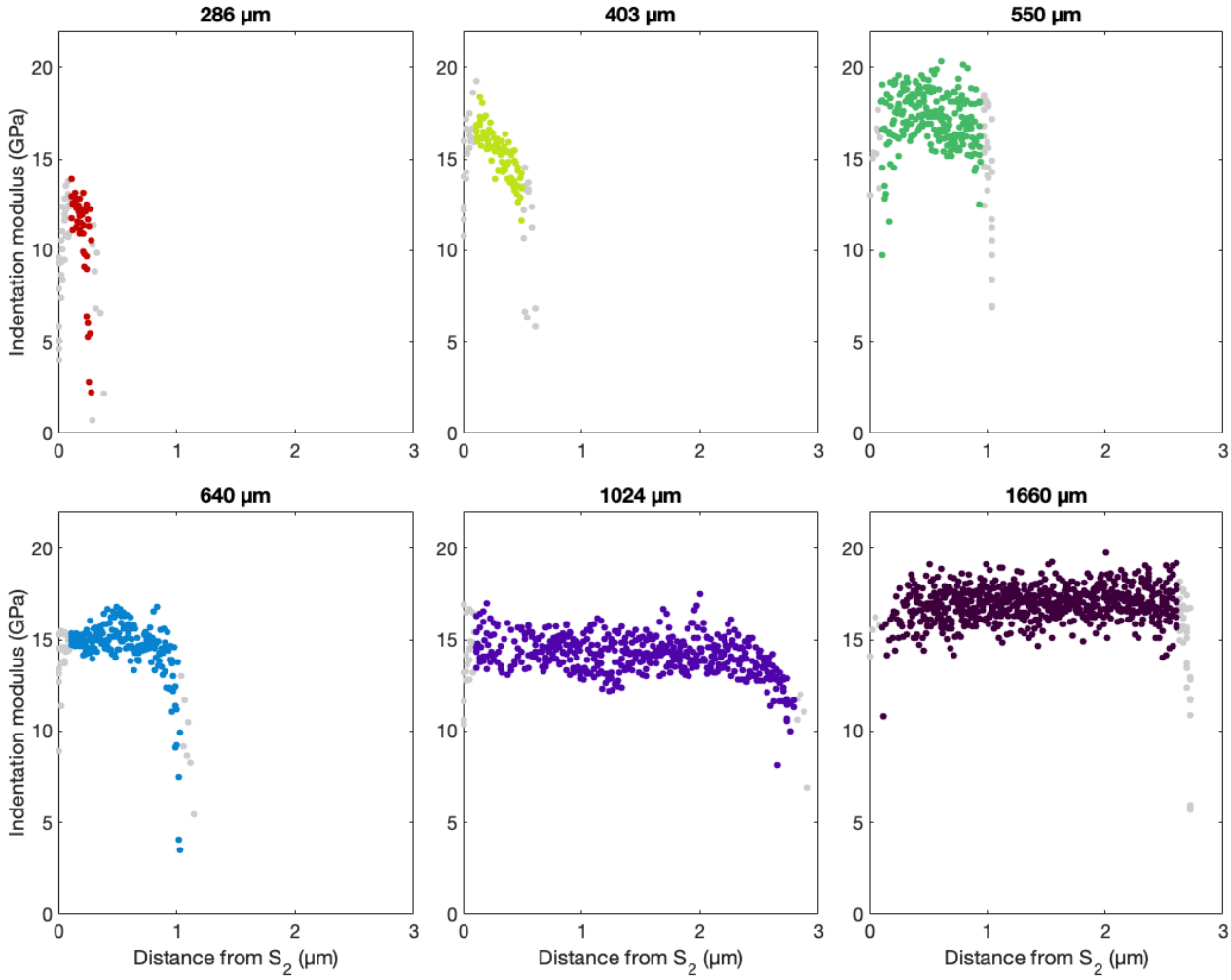

Fig. 5. Observation of the occurrence of a radial mechanical gradient during the maturation of the G-layer obtained by extracting radial profiles all around the cell axis in this layer and plotting them as a function of the distance from the S_2 layer for six different distances from the cambium (value given at the top of each graph). The first and last 100 nm were removed from each profile (data points in grey) to avoid any bias due to measurement edge effects.

Dynamics of global cell-wall layer thickening and stiffening

All the observations made above were also made in the 2nd and 3rd radial rows. Changes in the mode of the indentation modulus distribution in each layer (e.g., see Fig. S3) are shown in Fig. 6, as a function of the distance from the cambium, together with the relative thickness of each layer. In fig. 6, one point corresponds to one cell, whatever the radial rows, the continuous line corresponds to the mean trend adjusted on these points by a polynomial fit and the coloured ribbon to this fit shifted vertically by plus or minus the mean standard deviation on each layer of the cell wall.

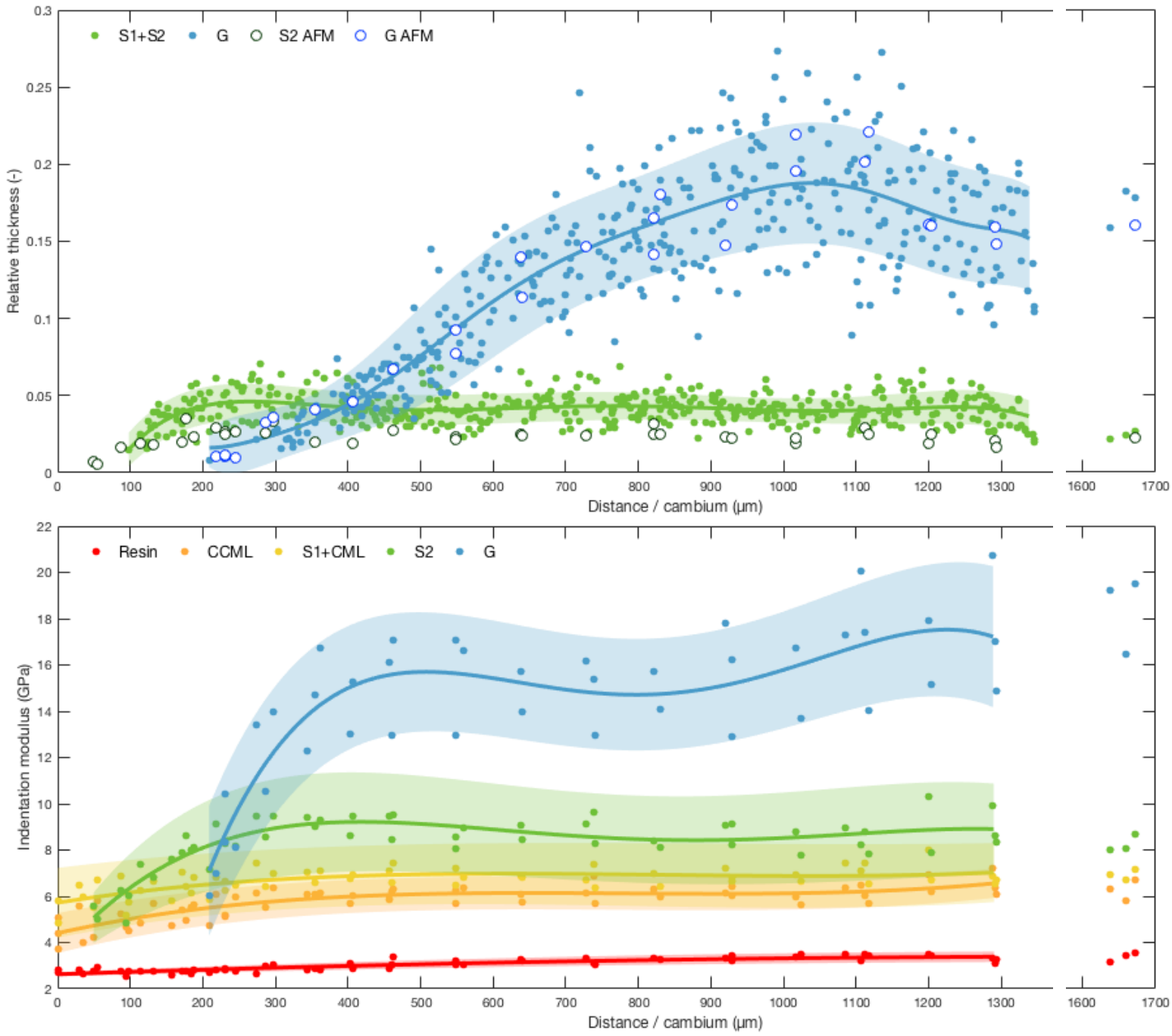
S1+S2
G
S2 AFM
G AFM
Relative thickness (-)
Distance / cambium (µm)
Resin
CCML
S1+CML
S2
G
Indentation modulus (GPa)
Distance / cambium (µm)

328

329 *Fig. 6. Variations in the relative thickness of the cell wall layers measured by optical microscopy*
330 *(coloured dots) and AFM (empty circles) (top) and mode of the indentation modulus distribution*
331 *(bottom), as a function of the distance from the cambium. The solid lines and the shaded areas show*
332 *the mean tendency and standard deviation adjusted on these points.*

333 In the case of the optical measurements of the thickness of the layers, it was not possible to separate
334 the S_1 and S_2 layers, unlike for the AFM measurements. The measurements of relative thickness made
335 by optical microscopy and AFM are consistent, but AFM enables detection of the appearance of the
336 cell wall layer and its thickening earlier than optical microscopy. The thickness of the S_2 alone
337 obtained by AFM is thus logically smaller than S_1+S_2 obtained by light microscopy. The relative
338 thickness of the S_2-layer increases until around 200 µm from the cambium then decreases a little
339 before reaching a stable value at a distance of around 500 µm from the cambium. The G-layers were
340 first detected close to 200 µm from the cambium. The relative thickness of the G-layer increased
341 linearly and stabilised near 1 000 µm. Thus, the relative thickness of S_2 was slightly higher before the
342 appearance of the G-layer.
343
344 A progressive increase in the indentation modulus of both the CCML (from 4.6±0.7 to 6.1±0.7 GPa)
345 and the S_1 layers (from 5.6±1.5 to 6.8±1.3 GPa) was observed until the end of the S_2 stiffening, at
346 around 350 µm from the cambium. The very first S_2-layers had indentation moduli of 5.1±1.4 GPa
347 and their stiffening and their thickening were initially synchronous. Later, when the S_2-layers reached
348 their final thickness, their indentation modulus continued to increase and finally reached a value of
349 8.7±2.0 GPa. All these layers continued to stiffen when the G layer began to thicken. In contrast, the
350 global stiffness of the G-layer was almost stable (at around 500 µm from the cambium) long before
351 it reached its final maximum thickness (at around 1 000 µm from the cambium).
352
353 As already mentioned, as these curves correspond to the mode of the indentation modulus distribution
354 (i.e., value at the maximum of the distribution or most frequent value, see Fig. S3), they do not reflect
355 the gradient observed at about 500 nm from the edge of the G-layer on the lumen side due to the
356 progressive maturation of a potentially freshly deposited sub-G-layer (Fig. 5). Furthermore, as shown
357 in Fig. 5, the thickness of the G-layer at 550 µm from the cambium is such that most of the G-layer
358 has completely stiffened, leading to the stabilised value of the indentation modulus reported in Fig. 6
359 for this distance from the cambium.

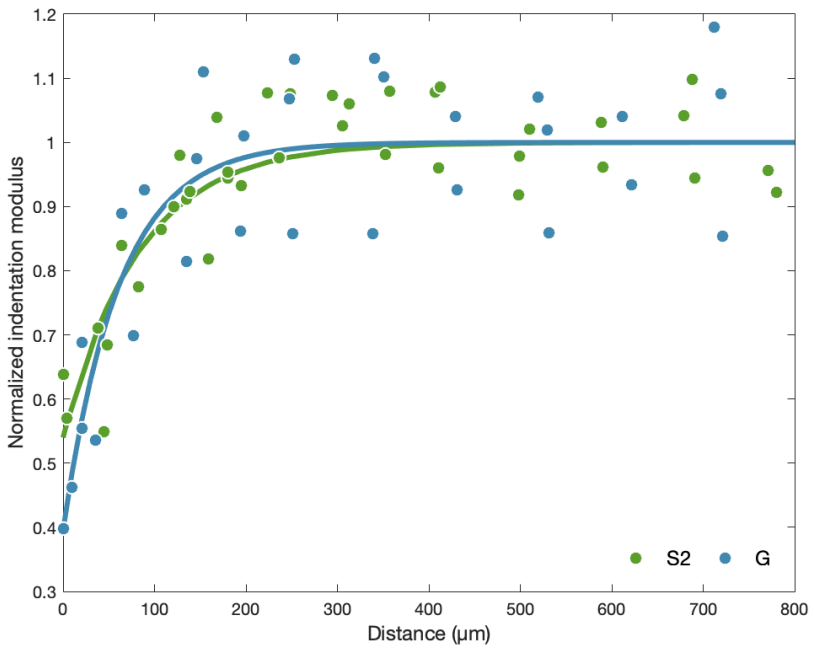

Fig. 7. Normalized indentation modulus of the S_2 and G-layers from Fig. 6 as a function of the distance from the cell where the layer concerned first appeared. The solid line corresponds to the mean value.

To compare the dynamics of the stiffening of the S_2 and G-layers, Fig. 7 shows the normalized indentation modulus (i.e., the modulus from Fig. 6 divided by its mean maximum value) as a function of the distance from the cell where the layer concerned first appeared (i.e., 50 µm from the cambium for S_2 and 230 µm for G-layers, Fig. 3). This figure shows that the dynamics of the two layers are quite similar, i.e., it took a distance of around 250 µm to reach their mature modulus. However, it appears to be faster for the G-layer as the change in modulus from the first deposited layer to the final mature one is larger.

Discussion

Our main results revealed: i) initial synchronous stiffening of the CML, S_1 and S_2-layers with the thickening of the S_2-layer, which continues a little after the S_2-layer has reached its final thickness while the G layer starts to develop; ii) initial global stiffening of the G-layer synchronous with its thicknening but stable global stiffness reached long before its final maximum thickness; iii) a stiffness gradient over about 500 nm on the lumen side in the developing G-layer with a softer sub-layer at the lumen edge about 100 nm in thickness.

Potential effects of sample preparation on the measurements

The different steps of sample preparation protocol made it impossible to keep the sample in its native *in planta* green state: we thus cannot rule out the possibility that modifications of the different layers of the cell wall during the ethanol exchange and resin embedding had some impacts on its mechanical properties but, for the reasons detailed below, we believe that we achieved a good compromise. Indeed, this preparation was necessary to ensure reliable mechanical measurements at small scale by AFM. Since all the measurements had to be comparable, this treatment minimised artifacts caused by roughness of the sample surface (Peaucelle, 2014). Indeed, mechanical measurements based on indentation require samples with a surface that is as flat as possible, compared to the radius of the AFM tip, to enable the use of reliable and simple contact mechanics models. These models are needed to extract the indentation modulus from the contact stiffness (Arnould and Arinero, 2015) or from the force-distance curves (Hermanowicz *et al.*, 2014). In addition, the AFM tip is very brittle and surface roughness has to be as low as possible to reduce the risk of tip wear or breakage: this is especially important in the present study where we had to perform many measurements using the same probe to limit measurement bias or drift. AFM measurements at such a small scale are only sensitive to the very near sample surface. Damage during preparation of the sample surface should therefore be reduced to the strict minimum. In addition, as we expected to find evidence for the existence of a mechanical gradient during the thickening of the cell wall layers, we had to begin taking measurements as close as possible to the cambium, where the cell wall is very thin and soft. This is only possible when the sample has been previously embedded to avoid, or at least reduce, deformation and damage during cutting and measurements. In addition, cell wall thickening progresses from the lumen side of the cell wall and, without embedding, measurements made close to the lumen would be highly modified due to border effects (Jakes *et al.*, 2008; Jakes *et al.*, 2009) unless the lumen is filled with a sufficiently stiff substance such as resin. Finally, these embedding steps reduce cell wall layer deformation during the cutting process and avoid swelling, detachment and collapse of the G-layer commonly observed after stress release (Clair *et al.*, 2005a; 2005b).

Other studies have shown that LR-White embedding resin has little impact on the mechanical properties of the cell wall due to very limited penetration into the cell wall of normal wood (Coste *et al.*, 2021) and *a priori* in the G-layers of tension wood (Arnould and Arinero, 2015) and of other similar fibre cell walls such as in flax (Arnould *et al*, 2017) and hemp (Coste *et al.*, 2020). What is more, the use of ethanol is expected to cause only slight deformation of the wall. For example, Chang *et al.* (2012) showed that ethanol dehydration produced longitudinal macroscopic shrinkage of only 0.2% and volumetric swelling of only 0.5%. It is possible to avoid ethanol dehydration by drying the

415 sample at moderate temperature just before embedding (Konnerth *et al.*, 2008). However, in the
416 present biomechanical context with the G-layer, such a drying step would lead to very significant
417 changes in the cell wall ultrastructure (such as mesoporosity collapse, Clair *et al.*, 2008).
418
419 The main impact of sample preparation on the mechanical properties of the cell wall is in fact its
420 potential effects on the moisture content of the different layers. Indeed, sample preparation probably
421 modified moisture content from a green state to close to an air-dry state. The effect of moisture
422 content on the mechanical properties of the different cell wall layers has already been measured by
423 nanoindentation in the cell corner middle lamella and the S_2 layer of different woody species using
424 samples that were embedded (Wagner *et al.*, 2015) or not (Bertinetti *et al.*, 2015; Meng *et al.*, 2015).
425 These studies revealed a similar trend with a reduction of the indentation modulus from one third to
426 one half for the S_2 layer and at least one half for the cell corner middle lamella, between an air-dry
427 and saturated state. A more recent study (Coste *et al.*, 2020), using AFM PF-QNM in similar
428 conditions to those used in our study, focused on the effect of the moisture content on the mechanical
429 properties of hemp sclerenchyma fibres (containing a thick G-layer with similar characteristics to
430 those of the tension wood G-layer) and xylem fibres. In their study, AFM measurements of all the
431 cell wall layers revealed no major differences between layers, with a reduction of the indentation
432 modulus of about one half when the relative humidity varied from 13% to 83%. If we extrapolate
433 these variations to our study, the indentation modulus values reported here are overestimated
434 compared to the values *in planta* but the relative differences observed between layers, or within a
435 layer (gradient), are most probably comparable to what happens in the tree.
436
437 ***Indentation modulus and its variations in the different layers of the cell wall***

438 We observed an increase in the indentation modulus of the embedding resin in the lumen, with
439 increased distance from the cambium, but it goes back to values measured in the cambial zone in the
440 normal wood (before tilting) cells lumen. The origin of this increase during fibre maturation is not
441 yet understood but is unlikely to be due to wear of the AFM tip as demonstrated by the repeatability
442 of the measurements in the cambial cells performed after measurements of each row, which were also
443 identical to those obtained at the end of all measurements in the lumen of the normal wood cells or
444 in the resin outside the sample. Stiffening thus appears to be associated with the change in the contents
445 of the lumen with the maturation of the fibres (as shown in Fig. 3). In cambial cells, the plasma
446 membrane and cytoplasm are bound to the inner part of the cell wall. Cambial cells are highly
447 vacuolated, and the large vacuole pushes the cell organelles outwards. There is therefore little material
448 inside the lumen (vacuole contents), which may explain why the indentation modulus measured in

the resin in the centre of cambial cells is close to that measured in normal wood cells that have lost all their cell contents. Finally, Table 1 shows that our LR-White indentation modulus values were the lowest, but were confirmed by nanoindentation. This is probably due to differences in the calibration procedure between laboratories or to the variability of the resin itself, as different grades (soft, medium, and hard) of this resin are available.

The values of the indentation modulus in the different layers and the embedding resin are consistent with the (rather scattered) AFM data or nanoindentation measurements of wood cell walls available in the literature (Eder *et al.*, 2013), although in the low range compared literature data on the G-layer of poplar or tension wood (see Table 1). These low values can probably be partly explained by the fact that the tree used in our study was young (less than 3-month old), and the juvenile wood it produced had a high microfibril angle (MFA) in the S_2-layer and low cellulose content (Luo *et al.*, 2021), and the fact that the cell used as an example in Fig. 2 was not fully mature. The values of the indentation modulus in the G-layer of a mature cell increased to around 18.3±3.1 GPa on average (see Fig. 6), a value similar to the literature data listed in Table 1.

Table 1. Comparison of the value of the indentation modulus (in GPa) in the different layers of mature wood fibres in our study and in the literature.

Reference	**LR-White resin (lumen)**	**ML (CC)**	**S_1**	**S_2**	**G**
This study, developing tension wood (740 µm, Figs. 2 and S2)	3.10±0.29	5.4±1.0	6.5±1.4	8.3±2.2	13.0±3.1
This study, mature tension wood (1660 µm, Fig. 3)	3.35±0.27	5.9±1.0	6.7±1.2	8.2±2.6	16.5±3.3
This study, mature normal wood (NW, Fig. 3)	2.99±0.21	7.5±1.2	8.2±3.1	16.9±5.5	n.a.
Normand *et al.* (2021) (poplar)	3.9±1.8	9.9±1.2	11.3±0.3	16.4±0.4	16.8±0.5
Clair *et al.* (2003) (oak, no embedding)	n.a.	5-7	8-9	9-10	10-12
Arnould and Arinero (2015) (chestnut)	3.5±1.5	6±0.5	n.a.	13±0.5	15±1.5
Liang *et al.* (2020) (poplar, no embedding)	n.a.	n.a.	6.89-10.48	10.57-14.61	11.13-18.5
Coste *et al.* (2021) (poplar)	4.5±0.9	10.7±2	16.0±3.8	18.2±3.5	n.a.

468 The low value obtained for the mature S_2-layer in the tension wood area compared to the value in
469 normal wood can be explained by a marked difference in MFA between the S_2-layers of normal wood
470 (with a low MFA and therefore a high indentation modulus) and the S_2-layers of tension wood (with
471 a high MFA and therefore a small indentation modulus, Eder *et al.*, 2013; Jäger *et al.*, 2011). To
472 explain this difference (equal to a factor of about 2) between the indentation moduli, we can roughly
473 estimate from published data that the MFA is around 5-10° in normal wood whereas it is 30-40° in
474 the S_2 of tension wood (Arnould and Arinero, 2015; Jäger *et al.*, 2011). This is also in agreement with
475 the value of MFA reported for the S_2-layer in tension wood for poplar by Goswami *et al.* (2008).
476 Likewise, the order of magnitude of the values of indentation modulus obtained for the different
477 layers of normal wood is in agreement with other literature data (Table 1).
478
479 ***Dynamics of global thickening and stiffening of the cell-wall layers***

480 The CCML, S1 and S_2-layers continued to stiffen while G-layer was developing (Fig. 6). This is in
481 agreement with the fact that the lignification of S_1, S_2-layers and CCML occurs during the formation
482 of the G-layer (Yoshinaga *et al.*, 2012). This lignification after the G-layer starts to thicken may be
483 explained by the presence of additional matrix material that has been transported through the existing
484 wall. Alternatively, some precursors may already be present and are used in biochemical reactions
485 that continue during the deposition of the G-layer. The effect of lignification on the mechanical
486 properties of the cell wall is not yet well understood, with different studies sometimes reporting
487 conflicting results, but recent studies tend to confirm the hypothesis that lignification mainly affects
488 the shear modulus and the strength of the matrix (Özparpucu *et al.*, 2017; 2019), with higher content
489 leading to a higher modulus and greater strength. As the indentation modulus is not only sensitive to
490 the longitudinal modulus but also to the transverse and shear moduli (Jäger *et al.*, 2011), which are
491 mainly influenced by the cell wall matrix, a change in the cell wall matrix properties due to
492 lignification causes a significative change in the indentation modulus, as already shown by
493 nanoindentation (Gindl et al., 2002). Finally, Fig. 7 shows that the stiffening dynamics appear similar
494 although faster in the G-layer than in the S_2-layers suggesting that the physical and chemical changes
495 or reactions at work during cell wall maturation are faster in the G-layer (e.g., microfibrils aggregation
496 or gelatinous matrix swelling, Alméras and Clair, 2016) than in the S_2-layer (e.g., lignification).
497
498 The fact that the thickness of the S_2-layer decreases slightly when the G-layer is starting to develop
499 has already been observed. For example, Abedini *et al.* (2015) reported that this is a common trend
500 throughout the growing season in both normal and tension wood of poplar trees. Moreover, the
501 changes and mature value of the relative thickness of the G and S_2 layers in Abedini *et al.* (2015),

Chang *et al.* (2015) and Clair *et al.* (2011) are similar to our measurements. We therefore assume that we can use the relative thickening of the different wall layer as a common spatial reference to link different studies. If we combine our results with those of previous studies, the G-layer appears to synchronously stabilise its thickness, whole indentation modulus (i.e., no more radial gradient), meso-pore size (Chang *et al.*, 2015) and cellulose tensile strain (Clair *et al.*, 2011) at the end of the maturation. These observations suggest that the different changes involved in the maturation process of the G-layer start, evolve and end at approximately the same fibre development stage. These physico-chemical observations now need to be coupled with biochemical analyses to better understand the mechanisms involved in G-layer maturation, and possibly to establish relations between matrix stiffening, bridging between microfibrils and wall compaction (Alméras and Clair, 2016; Gorshkova *et al.*, 2015; Mellerowicz and Gorshkova, 2012).

According to the radial profiles of the indentation modulus (Fig. 5), a smooth mechanical gradient occurs in immature G-layer on less than 0.5 µm on the lumen side with a small sublayer of about 100 nm. This sublayer appears to be as dense as the mature part of the layer and could be either a freshly deposited immature G-layer or part of the periplasmic area still bound to the layer. Indeed, periplasmic area, located between the inner part of the G-layer and the plasma membrane, is the scene of intense biochemical processes, see Fig. 2 in Pilate *et al.* (2004), Fig. 5 in Guedes *et al.* (2017) or Fig. 7 in Decou *et al.* (2020). In contrast, flax bast fibres exhibit a strong mechanical gradient with a thick immature, loose and soft G-layer, called G_n (Gorshkova and Morvan, 2006; Gorshkova *et al.*, 2010). Evidence for the presence of this thick G_n-layer has also been provided in flax xylem tension wood fibres (Petrova *et al.*, 2021). Interestingly, the indentation modulus of flax G-layers is similar to or even a little bit higher than that of mature poplar G-layers and the average indentation modulus of flax G_n-layers is comparable to that measured in immature poplar G-layers in fibres close to the cambium and to the inner sub-layers observed in more developed G-fibres.

Comparison with flax G-layer

The indentation modulus and adhesion force maps in the case of a typical developing flax fibre with a sharp transition between G and G_n layers (Arnould *et al.*, 2017; Goudenhooft *et al.*, 2018) are shown in Fig. 8. Several sublayers are observed as lamellae in the G_n, which exhibit indentation modulus and adhesion force similar to those of the G-layer. These lamellae are separated by bands whose indentation modulus is close to that of the resin, but with a lower adhesion force. This lamellar arrangement is not observed in poplar, even though ring lamellae structure of this type is sometimes discernible in the mature part of the G-layer (e.g., see cells at a distance of 548, 740, 830, 930, 1 024

and 1 660 µm µm from the cambium in Fig. 3 and Fig. S1). The most significant structure in the poplar G-layer appears as radial bands (e.g., see tension wood cells at a distance of more than 740 µm in Fig. 3). This pattern may reflect biological organisation, but we cannot exclude the possibility that it is the consequence of (slight) shrinkage of the G-layer during dehydration with ethanol (Fang *et al.*, 2007).

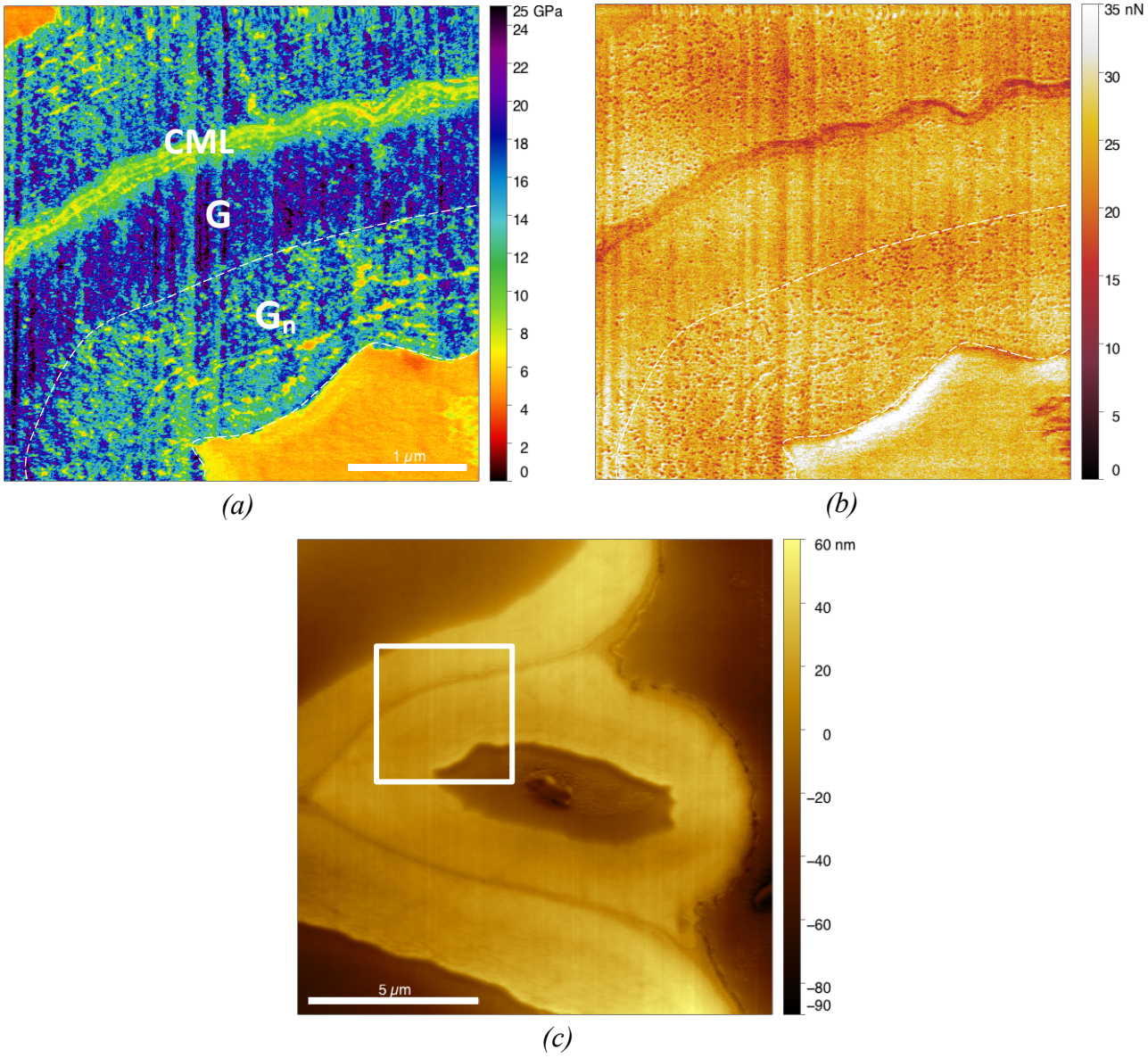

Fig. 8. Comparison of the G and G_n-layers in developing flax bast fibre (60 days, half height of the stem) adapted from Arnould et al. (2017): a) indentation modulus map and b) adhesion map corresponding to the white box in the topography image (c).

Note that it is impossible to compare the absolute value of adhesion forces obtained in the present study (Fig. 4b) with the values obtained in Arnould *et al.* (2017) (in Fig. 8b) as this force depends to

a great extent on the on the shape of the tip and on the surface roughness of the material, which were not the same (see for example the difference in adhesion forces of the embedding resin in the lumen in the two studies, even though the same resin was used). In conclusion, although the G-layer of tension wood and the G-layer of flax are biochemically, ultrastructurally and mechanically similar (Coste *et al.*, 2020; Petrova *et al.*, 2021), here it is clear that they differ in their development and maturation, as summarised in Fig. 9, with a thick, loose, multilayer G_n layer in flax that stiffens and densifies abruptly, whereas in poplar, there appears to be a thin, dense immature layer that stiffens gradually. Thus, immunohistochemical and G-layer specific marker gene expression analyses (Decou *et al.*, 2020; Guedes *et al.*, 2017), like those already performed on flax bast and xylem fibres (Petrova *et al.*, 2021), should be performed on the same sample to clarify the origin of these differences and to better understand the mechanisms underlying the maturation and development of poplar tension wood growth stress. Finally, all these results should be used to distinguish between different models of growth stress development in the case of tension wood (Alméras and Clair, 2016), to estimate the internal stress distribution within the G-layer and its consequences for macroscopic growth stress at the tree scale (Alméras *et al.*, 2009).

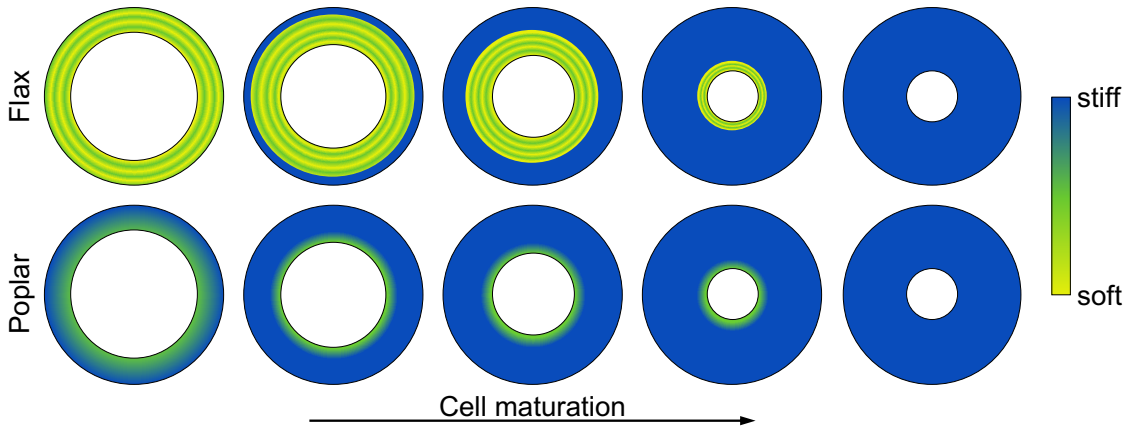

Fig. 9. Comparative scheme of the maturation (thickening and stiffening) of the G-layer of flax and poplar.

Acknowledgements

The authors are grateful to C. Assor (UMR IATE, Sup'Agro, INRAE Montpellier, France) for fruitful discussions and to D. Pellerin (ScienTec) for nanoindentation measurements. This work was performed in the framework of the project "StressInTrees" (ANR-12-BS09-0004) funded by the French National Research Agency (ANR).

Author contributions

OA participated in sample preparation, supervised and designed all the experiments and data analysis, performed some of them, and contributed to writing the original draft of the paper. MC performed some of the experiments and the data analysis, wrote the original draft of the paper. MR supervised and performed all the experiments. FL prepared the sample and contributed fruitful discussions to the data analysis. TA contributed to data analysis and to writing the original draft of the paper. GP contributed to data analysis. BC contributed to data analysis, conceptualised and supervised the whole project. All the authors reviewed and edited the paper and approved the final version.

Data availability statements

The datasets used and/or analysed during the current study are available from the corresponding author upon reasonable request.

References

Abedini R, Clair B, Pourtahmasi K, Laurans F, Arnould O. 2015. Cell wall thickening in developing tension wood of artificially bent poplar trees. IAWA Journal **36**, 44-57.

Alméras T, Gril J, Yamamoto H. 2005. Modelling anisotropic maturation strains in wood in relation to fibre boundary conditions, microstructure and maturation kinetics. Holzforschung **59**, 347-353.

Alméras T, Clair B, Gril J. 2009. The origin of maturation stress in tension wood: using a micro-mechanical model to discriminate between hypothetic mechanism. In: COST E50 final conference "Systems Biology for Plant Design", Wageningen, The Netherlands, 09-11.07.2009. https://hal.archives-ouvertes.fr/hal-00797122.

Alméras T, Fournier M. 2009. Biomechanical design and long-term stability of trees: Morphological and wood traits involved in the balance between weight increase and the gravitropic reaction. Journal of Theoretical Biology **256**, 370-381.

Alméras T, Clair B. 2016. Critical review on the mechanisms of maturation stress generation in trees. Journal of the Royal Society Interface **13**, 20160550.

Alméras T, Jullien D, Gril J. 2018. Modelling, evaluation and biomechanical consequences of growth stress profiles inside tree stems. In: Geitmann A, Gril J, eds. Plant biomechanics: From structure to function at multiple scale. Berlin: Springer, 21-48.

Archer RR. 1986. Growth stresses and strains in trees. In: Timell TE, ed. Springer Series in Wood Science, Berlin Heidelberg: Springer.

Arnould O, Arinero R. 2015. Towards a better understanding of wood cell wall characterisation with contact resonance atomic force microscopy. Composites: Part A **74**, 69-76.

Arnould O, Siniscalco D, Bourmaud A, Le Duigou A, Baley C. 2017. Better insight into the nano-mechanical properties of flax fibre cell walls. Industrial Crops and Products **97**, 224-228.

Bertinetti L, Hangen UD, Eder M, Leibner P, Fratzl P, Zlotnikov I. 2015. Characterizing moisture-dependent mechanical properties of organic materials: humidity-controlled static and dynamic nanoindentation of wood cell walls. Philosophical Magazine **95**, 1992-1998.

Casdorff K, Keplinger T, Burgert I. 2017. Nano-mechanical characterization of the wood cell wall

by AFM studies : comparison between AC- and QI mode. Plant Methods **13**, 60.

Casdorff K, Keplinger T, Rüggeberg M, Burgert I. 2018. A close-up view of the wood cell wall ultrastructure and its mechanics at different cutting angles by atomic force microscopy. Planta doi: 10.1007/s00425-018-2850-9.

Chang SS, Clair B, Ruelle J, Beauchêne J, Di Renzo F, Quignard F, Zhao GJ, Yamamoto H, Gril J. 2009. Mesoporosity as a new parameter in understanding of tension stress generation in trees. Journal of Experimental Botany 60, 3023-3030.

Chang SS, Quignard F, Di Renzo F, Clair B. 2012. Solvent polarity and internal stresses control the swelling behavior of green wood during dehydration in organic solution. BioResources **7**, 2418-2430.

Chang SS, Quignard F, Alméras T, Clair B. 2015. Mesoporosity changes from cambium to mature tension wood: a new step toward the understanding of maturation stress generation in trees. New Phytologist **205**, 1277-1287.

Clair B, Arinero R, Leveque G, Ramonda M, Thibaut B. 2003. Imaging the mechanical properties of wood cell wall layers by atomic force modulation microscopy. IAWA Journal **24**, 223-230.

Clair B, Gril J, Baba K, Thibaut B, Sugiyama J. 2005a. Precaution for the structural analysis of the gelatinous layer in tension wood. IAWA Journal **26**, 189-195.

Clair B, Thibaut B, Sugiyama J. 2005b. On the detachment of gelatinous layer in tension wood fibre. Journal of Wood Science **51**, 218-221.

Clair B, Gril J, Di Renzo F, Yamamoto H, Quignard F. 2008. Characterization of a gel in the cell wall to elucidate the paradoxical shrinkage of tension wood. Biomacromolecules **9**, 494-498.

Clair B, Alméras T, Pilate G, Jullien D, Sugiyama J, Riekel C. 2011. Maturation stress generation in poplar tension wood studied by synchrotron radiation micro-diffraction. Plant Physiology **155**, 562-570.

Coste R, Pernes M, Tetard L, Molinari M, Chabbert B. 2020. Effect of the interplay of composition and environmental humidity on the nanomechanical properties of hemp fibers. ACS Sutainable Chemistry and Engineering **8**, 6381-6390.

Coste R, Soliman M, Bercu NB, Potiron S, Lasri K, Aguié-Béghin V, Tetard L, Chabbert B, Molinari M. 2021. Unveiling the impact of embedding resins on the physicochemical traits of wood cell walls with subcellular functional probing. Composites Science and Technology **201**, 108485.

Côté WA, Day AC, Timell TE. 1969. A contribution to the ultrastructure of tension wood fibers. Wood Science and Technology **3**, 257-271.

Dadswell HE, Wardrop AB. 1955. The structure and properties of tension wood. Holzforschung **9**, 97-104.

Decou R, Labrousse P, Béré E, Fleurat-Lessard P, Krausz P. 2020. Structural features in tension wood and distribution of wall polymers in the G-layer of in vitro grown poplars. Protoplasma **257**, 13-29.

Derjaguin BV, Muller VM, Toporov, YP. 1975. Effect of contact deformations on the adhesion of particles. Journal of Colloid and Interface Science **53**, 314-326.

Eder M, Arnould O, Dunlop JWC, Hornatowska J, Salmén L. 2013. Experimental micromechanical characterisation of wood cell walls. Wood Science and Technology **47**, 163-182.

Fahlén J, Salmén L. 2002. On the lamellar structure of the tracheid cell wall. Pant Biology **4**, 339-345.

Fang CH, Clair B, Gril J, Alméras T. 2007. Transverse shrinkage in G-fibers as a function of cell

wall layering and growth strain. Wood Science and Technology **41**, 659-671.

Fang CH, Clair B, Gril J, Liu S. 2008. Growth stresses are highly controlled by the amount of G-layer in poplar tension wood. IAWA Journal **29**, 237-246.

Fournier M, Alméras T, Clair B, Gril J. 2014. Biomechanical action and biological functions. In: Gardiner B, Barnett J, Saranpää P, Gril J, eds. The biology of reaction wood. Berlin: Springer, Berlin, 139-169.

Ghislain B, Nicolini EA, Romain R, Ruelle J, Yoshinaga A, Alford MH, Clair B. 2016. Multilayered structure of tension wood cell walls in *Salicaceae sensu lato* and its taxonomic significance. Botanical Journal of the Linnean Society **182**, 744-756.

Ghislain B, Clair B. 2017. Diversity in organisation and lignification of tension wood fibre walls – a review. IAWA Journal **38**, 245-265.

Gindl W, Gupta HS, Grünwald C. 2002. Lignification of spruce tracheid secondary cell walls related to longitudinal hardness and modulus of elasticity using nano-indentation. Canadian Journal of Botany **80**, 1029-1033.

Gorshkova TA, Morvan C. 2006. Secondary cell-wall assembly in flax phloem fibres: role of galactans. Planta **223**, 149-158.

Gorshkova TA, Gurjanov OP, Mikshina PV, Ibragimova NN, Mokshina NE, Salnikov VV, Ageeva MV, Amenitskii SI, Chernova TE, Chemikosova SB. 2010. Specific type of secondary cell wall formed by plant fibers. Russian Journal of Plant Physiology **57**, 328-341.

Gorshkova TA, Mokshina N, Chernova T, Ibragimova N, Salnikov V, Mikshina P, Tryfona T, Banasiak A, Immerzeel P, Dupree P, Mellerowicz EJ. 2015. Aspen tension wood fibers contain β-(1→4)-galactans and acidic arabinogalactans retained by cellulose microfibrils in gelatinous walls. Plant Physiology **169**, 2048-2063.

Goswami L, Dunlop JWC, Jungnikl K, Eder M, Gierlinger N, Coutand C, Jeronimidis G, Fratzl P, Burgert I. 2008. Stress generation in the tension wood of poplar is based on the lateral swelling power of the G-layer. The Plant Journal **56**, 531-538.

Goudenhooft C, Siniscalco D, Arnould O, Bourmaud A, Sire O, Gorshkova T, Baley C. 2018. Investigation of the mechanical properties of flax cell walls during plant development: the relation between performance and cell wall structure. Fibers **6** doi: 10.3390/fib6010006.

Grozdits GA, Ifju G. 1969. Development of tensile strength and related properties in differentiating coniferous xylem. Wood Science 1, 137-147.

Guedes FTP, Laurans F, Quemener B, Assor C, Lainé-Prade V, Boizot N, Vigouroux J, Lesage-Descauses MC, Leplé JC, Déjardin A, Pilate G. 2017. Non-cellulosic polysaccharide distribution during G-layer formation in poplar tension wood fibers: abundance of rhamnogalacturonan I and arabinogalactan proteins but no evidence of xyloglucan. Planta **246**, 857-878.

Huang Y, Fei B, Wei P, Zhao C. 2016. Mechanical properties of bamboo fiber cell walls during the culm development by nanoindentation. Industrial Crops and Products **92**, 102-108.

Hermanowicz P, Sarna M, Burda K, Gabrys H. 2014. AtomicJ: An open source software for analysis of force curves. Review of Scientific Instruments **85**, 063703.

Hock CW. 1942. Microscopic structure of flax and related bast fibres. Journal of Research of the National Bureau of Standards **29**, 41-50.

Jäger A, Bader T, Hofstetter K, Eberhardsteiner J. 2011. The relation between indentation modulus, microfibril angle, and elastic properties of wood cell walls. Composites Part A: Applied Science and Manufacturing **42**, 677-685.

Jakes JE, Frihart CR, Beecher JF, Moon RJ, Stone DS. 2008. Experimental method to account

for structural compliance in nanoindentation measurements. Journal of Materials Research **23**, 1113-1127.

Jakes JE, Frihart CR, Beecher JF, Moon RJ, Resto P, Melgarejo Z, Suárez OM, Baumgart H, Elmustafa AA, Stone DS. 2009. Nanoindentation near the edge. Journal of Materials Research **24**, 1016-1031.

Johnson KL. 1987. Contact mechanics. Cambridge University Press.

Johnson KL, Greenwood JA. 1997. An adhesion map for the contact of elastic spheres. Journal of Colloid Interface Science **192**, 326-333.

Konnerth J, Harper D, Lee SH, Rials TG, Gindl W. 2008. Adhesive penetration of wood cell walls investigated by scanning thermal microscopy (SThM). Holzforschung **62**, 91-98.

Kozlova L, Petrova A, Ananchenko B, Gorshkova T. 2019. Assessment of primary cell wall nanomechanical properties in internal cells of non-fixed maize roots. Plants **8**, 172.

Liang R, Zhu YH, Yang X, Gao JS, Zhang YL, Cai LP. 2020. Study on the ultrastructure and properties of gelatinous layer in poplar. Journal of Materials Science **56**, 415–427.

Luo L, Zhu Y, JGui J, Yin T, Luo W, Liu J, Li L. 2021. A comparative analysis of transcription networks active in juvenile and mature wood in Populus. Frontiers in Plant Science **12**, 675075.

Mellerowicz EJ, Gorshkova TA. 2012. Tensional stress generation in gelatinous fibres: a review and possible mechanism based on cell-wall structure and composition. Journal of Experimental Botany **63**, 551-565.

Meng Y, Xia Y, Young TM, Cai Z, Wang S. 2015. Viscoelasticity of wood cell walls with different moisture content as measured by nanoindentation. RSC Avances **5**, 47538.

Moulia B, Coutand C, Lenne C. 2006. Posture control and skeletal mechanical acclimation in terrestrial plants: implications for mechanical modeling of plant architecture. American Journal of Botany **93**, 1477-1489.

Muraille L, Aguié-Béghin V, Chabbert B, Molinari M. 2017. Bioinspired lignocellulosic films to understand the mechanical properties of lignified plant cell walls at nanoscale. Scientific Reports **7**, 44065.

Nair SS, Wang S, Hurley DC. 2010. Nanoscale characterization of natural fibers and their composites using contact-resonance force microscopy. Composites: Part A **41**, 624-631.

Niklas KJ. 1992.Plant biomechanics. An engineering approach to plant form and function. Chicago: University of Chicago Press.

Normand AC, Charrier AM, Arnould O, Lereu AL. 2021. Influence of force volume indentation parameters and processing method in wood cell walls nanomechanical studies. Scientific Reports **11**, 5739.

Okumura S, Harada H, Saiki H. 1977. Thickness variation of the G-layer along a mature and a differentiating tension wood fiber in *Populus euramericana*. Wood Science and Technology **11**, 23-32.

Okuyama T, Yamamoto H, Yoshida M, Hattori Y, Archer RR. 1994. Growth stresses in tension wood: role of microfibrils and lignification. Annales des Sciences Forestières **51**, 291-300.

Onaka F. 1949. Studies on compression and tension wood. Wood Research **1**, 1-88.

Özparpucu M, Rüggeberg M, Gierlinger N, Cesarino I, Vanholme R, Boerjan W, Burgert I. 2017. Unravelling the impact of lignin on cell wall mechanics: a comprehensive study on young poplar trees downregulated for CINNAMYL ALCOHOL DEHYDROGENASE (CAD). The Plant Journal **91**, 480-490.

Özparpucu M, Gierlinger N, Cesarino I, Burgert I, Boerjan W, Rüggeberg M. 2019. Significant influence of lignin on axial elastic modulus of poplar wood at low microfibril angles under wet conditions. Journal of Experimental Botany **70**, 4039-4047.

Peaucelle A. 2014. AFM-based mapping of the elastic properties of cell walls: at tissue, cellular, and subcellular resolutions. Journal of Visualized Experiments **89**, e51317.

Petrova A, Kozlova L, Gorshkov O, Nazipova A, Ageeva M, Gorshkova T. 2021. Cell wall layer induced in xylem fibers of flax upon gravistimulation is similar to constitutively formed cell walls of bast fibers. Frontiers in Plant Science **12**, 660375.

Pilate P, Déjardin A, Laurans F, Leplé JC. 2004. Tension wood as a model for functional genomics of wood formation. New Phytologist **164**, 63-72.

Pot G, Coutand C, Le Cam JB, Toussaint E. 2013a. Experimental study of the mechanical behaviour of thin slices of maturating green poplar wood using cyclic tensile tests. Wood Science and Technology **47**, 7-25.

Pot G, Toussaint E, Coutand C, Le Cam JB. 2013b. Experimental study of the viscoelastic properties of green poplar wood during maturation. Journal of Materials Science **48**, 6065-6073.

Pot G, Coutand C, Toussaint E, Le Cam JB, Saudreau M. 2014. A model to simulate the gravitropic response and internal stresses in trees, considering the progressive maturation of wood. Trees doi: 10.1007/s00468-014-1033-y

Richardson KC, Jarett L, Finke EH. 1960. Embedding in epoxy resins for ultrathin sectioning in electron microscopy. Stain Technology **35**, 313-323.

Scurfield G. 1973. Reaction wood: its structure and function. Science **179**, 647-655.

Sell J, Zimmermann T. 1998. The fine structure of the cell wall of hardwoods on transverse-fracture surfaces. European Journal of Wood and Wood Products **56**, 365-366.

Sudharshan Phani P, Oliver WC. 2019. A critical assessment of the effect of indentation spacing on the measurement of hardness and modulus using instrumented indentation testing. Materials and Design **164**, 107563.

Thibaut B, Gril J, Fournier M. 2001. Mechanics of wood and trees: some new highlights for an old story. Comptes Rendus de l'Académie des Sciences – Series IIB **329**, 701-716.

Wagner L, Bader TK, De Borst K. 2014. Nanoindentation of wood cell walls: effects of sample preparation and indentation protocol. Journal of Materials Science **49**, 94-102.

Wang X, Ren H, Zhang B, Fei B, Burgert I. 2012. Cell wall structure and formation of maturing fibres of moso bamboo (Phyllostachys pubescens) increase buckling resistance. Journal of the Royal Society Interface **9**, 988-996.

Xu D, Liechti KM, Ravi-Chandar K. 2007. On the modified Tabor parameter for the JKR–DMT transition in the presence of a liquid meniscus. Journal of Colloid and Interface Science **315**, 772-785.

Yamamoto H. 1998. Generation mechanism of growth stresses in wood cell walls: roles of lignin deposition and cellulose microfibril during cell wall maturation. Wood Science and Technology **32**, 171–182.

Yoshinaga A, Kusumoto H, Laurans F, Pilate G, Takabe K. 2012. Lignification in poplar tension wood lignified cell wall layers. Tree Physiology **32**, 1129-1136.

Zhang SY, Fei BH, Wang CG. 2016. Effects of chemical extraction treatments on nano-scale mechanical properties of the wood cell wall. BioResources **11**, 7365-7376.